The Effect of Heat Treatment on Microstructure and Tensile Properties of Ti-10V-2Fe-3Al

Terlinde, Duerig, Williams

Titanium '80 Science and Technology - Proceedings of the 4th Int'l Conference on Titanium
(eds.) H. Kimura, O. Izumi
Vol. 2
pp. 1571-1581

1980

THE EFFECT OF HEAT TREATMENT ON MICROSTRUCTURE AND TENSILE
PROPERTIES OF Ti-10V-2Fe-3Al

G. T. Terlinde, T. W. Duerig, and J. C. Williams

Carnegie-Mellon University, Pittsburgh, PA U.S.A.

Introduction

The use of high strength titanium alloys is still dominated by α and
$\alpha+\beta$ alloys such as Ti-5Al-2.5Sn and Ti-6Al-4V. However, there now is an in-
creasing interest in a class of alloys known as metastable β-Ti alloys.
These alloys are so-named because they can contain 100% metastable β-phase
upon quenching to room temperature. Such alloys also can develop very high
strength levels during aging. Beside excellent strength to density and good
strength to toughness combinations, the β-Ti alloys exhibit a highly improved
deep hardenability for thick section applications. In addition to these ad-
vantages, most of these alloys exhibit considerable flexibility in strength
and a wide range of microstructures.

Among the more attractive β-alloys is the relatively new alloy Ti-10V-
2Fe-3Al (Ti-10-2-3). This alloy has a slightly higher Young's modulus, a
lower density and a less sluggish age hardening response than many of the
other β-alloys[5,6]. Much work has already been done to develop the manu-
facturing techniques and forging conditions for achieving attractive tensile
properties as well as fracture toughness and fatigue properties of Ti-10-2-3
[7-12]. However, only a limited amount of work has been done to systematically
change heat treatments after processing and to relate the different micro-
structures to the corresponding mechanical properties because the final prop-
erties depend both on the processing history and on the subsequent heat treat-
ments.

From earlier studies it is known that the morphology of the α-phase
(primary α, secondary α, and grain boundary α) as well as its volume fraction
can influence the mechanical properties in this alloy as well as in other
β-Ti alloys[1-4,9,11,13-18]. The main goal of this study was to establish a
variety of microstructures with a wide range of yield stresses for a fixed
forging condition with globular primary α. Using these, a comparison of the
other mechanical properties was made. In addition, a limited study has been
performed on material with a different forging history which resulted in
elongated primary α. Some microstructures from forgings which differ only in
primary α morphology have been tested. This allows some conclusions about
the influence of the primary α morphology on mechanical properties.

Experimental Methods

The majority of the Ti-10-2-3 alloy used in this study was supplied by
TIMET (Heat #P1452) as hot rolled plate. It had been thermomechanically
processed starting in the β-phase field with a final working step in the
($\alpha+\beta$) field starting from 730°C. The β-transus was determined as 805°C ± 3°C.
The alloy contained (by weight) 10.3%V, 2.2%Fe, 3.2%Al, 0.15%O, 0.009%N and
0.016%C, balance Ti. The other material was in the form of pancake forgings

which were worked in the β-field with a finish upset in the (α+β) field (774°C). The β-transus of this alloy was slightly lower than that of the plate. For heat treatments above 600°C, specimens were wrapped in Ta foil and vacuum encapsulated. Most of the heat treatments below 600°C were performed in a liquid nitrate salt bath.

Specimens for optical microscopy were electropolished in a solution of 5% H_2SO_4 in methanol at room temperature at a voltage of 21V. The etchant consisted of equal parts of 10% oxalic acid and 1% HF aqueous solutions.

Thin foils for transmission electron microscopy (TEM) were prepared in a twin jet electropolishing unit with an electrolyte of 59% methanol, 35% butanol and 6% perchloric acid cooled to -50°C. A voltage of 12-15V was used.

Tensile tests have been performed on electropolished and etched cylindrical specimens with a diameter of 6.4mm and 32mm gage length using an Instron testing machine with a clip-on extensometer. The tests were carried out in the L-direction of the plate at a strain rate of $5.5 \times 10^{-4} sec^{-1}$. The fracture surfaces of the tensile specimens have been studied by scanning electron microscopy (SEM).

Results

I. Microstructures

The microstructures studied here have been chosen using the results of a recent investigation of the phase transformation behavior of this alloy[19]. Therefore, the microstructural aspects of this work will only be briefly described here. A schematic phase diagram of a β-alloy (Fig. 1) is useful to illustrate the heat treatments we performed and the resulting microstructures. All heat treatments consisted of an elevated temperature solution treatment (ST) followed by a lower temperature aging treatment. Solution treating above the β-transus, e.g. at 850°C, leads to a recrystallized β-phase with equiaxed grains. The upper optical micrograph in Figure 1 illustrates this structure. Numerous inclusions are also visible. Solution treating in the two phase α+β field, in this case between 700°C and 780°C (see upper shaded area in Figure 1), results in a matrix of β-phase containing coarse, almost equiaxed primary α ($α_p$) particles. The lower micrograph in Figure 1 shows a typical (α+β) ST microstructure. The $α_p$ volume fraction decreases with increasing solution treatment temperature, here from 30% at 725°C to 0% at 805°C (the β-transus). This material also contains a fine subgrain structure which is stabilized by primary α. Poorly defined, pancake-like grains can be seen at low magnifications. These probably are due to the working history.

The solution treatments were followed by aging at temperatures between 200°C and 500°C (see lower shaded area in Fig. 1). Between about 200°C and 450°C the metastable ω-phase forms which transformed after sufficiently long aging times to blocky α-phase precipitates (Fig. 2a). This α is present as a uniform distribution of very small plates (length ~ 1000-1500Å, thickness 150 ~ 300Å). Above 400°C a second type of α-phase forms directly in an autocatalytic manner. This α has a much higher aspect ratio than the aforementioned α, typical dimensions were 3μm-8μm in length and a thickness of ~ 0.1μm (Fig. 2b). When aging above 400°C both the aging temperature and the rate of heating to the aging temperature affect the precipitation reaction. Heating rapidly to the aging temperature results in the autocatalytic reaction, whereas heating slowly leads first to ω formation during heating and

then to the finer α plates which replace the ω during holding at temperature. These differences have a marked influence on the mechanical properties as will be shown later.

Especially in the α-aged conditions subgrain boundary α and grain bound-ary α-phase has been observed which is illustrated by TEM micrographs in Figures 2c and 2d, respectively (arrows). Figure 2e shows ω-particles in a TEM dark field micrograph.

II.   Mechanical Properties

These results will be divided into the ($\alpha+\beta$) ST plus α-aged and the β-ST plus α-aged conditions to simplify presentation.   A limited number of tests were also performed on ω-aged specimens.   These results will be described also.

a.   ($\alpha+\beta$) ST plus α-aged conditions – It is well known that strengthening during aging is mainly due to the small secondary α precipitates[4,15] and the strength level is controlled by the size and volume fraction of these precip-itates.   On this basis, we have varied the yield stress in two ways, as de-scribed below.

First, we started with microstructures which had varying volume fractions of equiaxed α_p (from 0% to 30%) and which have been aged to the maximum yield strength attainable at a constant aging temperature of 500°C.   In this case, the volume fraction of secondary α increases as the amount of primary α de-creases.   Figure 3 shows the yield stress $\sigma_{0.2}$, the true fracture stress σ_F (after Bridgeman correction), and the true fraction strain ε_F as a function of the solution treatment temperature or volume fraction of primary α.   The yield stress can be increased from 1030MPa (149 ksi) to about 1350MPa (196 ksi) by decreasing the volume fraction of α_p from 30% (725°C) to 0% (805°C), however this causes the true fracture strain to drop from 0.99 to 0.05.   The true fracture stress, however, shows no significant change except a small decrease for specimens solution treated close to and above the β-transus. The values are between 1500-1550MPa (217-225 ksi).

Second, we studied microstructures with a constant α_p content of 10%, but with changing morphologies and also volume fractions of the secondary α-phase.   This was achieved by solution treating at 780°C ($\sim$ 10% primary α) and isothermally aging.   We have chosen an aging temperature of 500°C, which produces yield stress levels around 180-200 ksi, which also are commercially interesting.   Figure 4 illustrates the aging response; the yield stress is plotted versus aging time.   We have tested conditions where the specimens were heated rapidly (liquid salt) as well as slowly (air furnace), in order to assess the heating rate effect on the secondary α-phase.   Both conditions show a peak in yield stress, however the slowly heated specimens, with the smaller particles, show significantly higher values for all aging times. For example, after 1 hr the air aged condition has a yield stress of 1445MPa (209 ksi), while the salt bath aged condition shows only 1202MPa (175 ksi) (see also conditions III and IV in Table 1).   The yield stress difference be-comes smaller after longer aging times.   Figure 4 also contains the true fracture strain for the slowly heated and isothermally aged conditions.   At peak strength the true fracture strain, ε_F, passes through a minimum of 0.09 (with an elongation to fracture of e_F = 2.6%) and rises to 0.55 (e_F = 10.4%) at 1250MPa (181 ksi) yield stress.

For some microstructures with a constant volume fraction of primary α different aging temperatures have been chosen which resulted in increased

yield stresses for the lower aging temperature (see conditions I. and II in Table 1). This step seems to be interesting in order to achieve a most wide variety of primary α and secondary α combinations and the corresponding yield stress and ductility response. Possibly a more interesting way to use different aging temperatures was to age microstructures with different volume fractions of α_p to a comparable yield stress (see conditions II and III in Table 1). A microstructure with 30% α_p aged at 370°C to 1246MPa (180 ksi), for example, shows a true fracture strain of 0.19, while a condition with only 10% α_p aged at 500°C to a comparable yield stress has a much higher fracture strain of 0.63.

   b. β-ST plus α-aged conditions - The β-ST solution treated and α-aged microstructures were characterized by equiaxed β-grains with grain boundary α and secondary α within the grains. The main aging temperature used for a comparison with the (α+β) ST plus α-aged conditions was 500°C. Since aging in air led to macroscopic embrittlement, salt bath aging was performed which led to coarser secondary α particles and lower yield stresses. As expected from the aging response of the microstructures with 10% α_p (see Fig. 4), overaging is observed; the peak yield stress is higher due to the increased volume fraction of secondary α. The fracture strain passes through a minimum of 0.03 at the peak yield stress of about 1370MPa (199 ksi). Overaging to 1200MPa increases the fracture strain to about 0.17. The true fracture stress is between 1510MPa and 1440MPa, the slight decrease with increasing aging time is probably within experimental scatter. Aging in salt at lower temperatures such as 400°C has an embrittling effect similar to aging in air at 500°C. However, in this case, the embrittlement probably is due to an increased volume fraction of secondary α instead of a fine particle size.

   In addition to the above, we have studied several ω-aged conditions in the (α+β) ST and β-ST material. These conditions have been described to a limited extent elsewhere recently[19], but the results are summarized here because they complement the α-aged results. It is possible to reach the same strength levels as the α-aged conditions aging by ω-phase. Especially in the high strength conditions around 1250MPa (181 ksi) the ω-aged specimens consistently exhibit lower ductilities than the α-aged conditions (compare conditions II, III, V with VI in Table 1). In the low strength region (yield stress values of ∿965MPa (140 ksi), the ω-aged conditions can show ductilities comparable to the α-aged conditions. The uniform elongations, as well as the tensile strengths, however, are always smaller.

   Beside strength control, the most important goal of this study was to investigate the tensile ductility or, more generally, the fracture behavior of the different types of microstructures at different strength levels. For this purpose it is very useful to illustrate the results in a diagram where the yield stress $\sigma_{0.2}$ is plotted versus the true fracture strain ε_F or reduction in area RA, respectively (see Fig. 5). We organized the data in Figure 5 by forming groups of microstructures each having a constant volume fraction of α_p and having been aged to different yield stresses. From such a diagram it is, for example, possible to find out 1) which correlation exists between $\sigma_{0.2}$ and ε_F for such a group and 2) if the ductilities of the various groups are different at comparable yield stresses. From our diagram we found the following results: 1) At a constant volume fraction of α_p, an increase in yield stress leads to a reduction in ductility. This well-known tendency is illustrated by trend lines. 2) For the (α+β) St plus α-aged microstructures an increase in primary α volume fraction leads to a reduction in ductility at comparable yield stresses. This tendency is observed over the whole yield stress range investigated. At about 1250MPa (∿ 181 ksi) yield stress, for

example, the microstructure with 10% primary α shows a true fracture strain of about 0.5 compared to 0.18 for the condition with 30% primary α and the same yield stress. 3) The β-ST plus α-aged microstructures show lower ductilities than the $\alpha+\beta$ ST plus aged structures for all yield stresses investigated. The trend line for β-ST conditions is steeper than those of the ($\alpha+\beta$) ST plus α-aged conditions which means that there is also less ductility gain by reducing the yield stress. At about 1250MPa (181 ksi) yield stress, however, the ductility is close to that of a microstructure with 30% α_p. 4) For the forging (pancake) with elongated α_p, the ductilities of equivalent ($\alpha+\beta$) ST plus α-aged conditions compared to the plate forging with globular α_p are lower at comparable yield stresses. At 1300MPa (188 ksi), for example, the microstructure with $\sim$ 15% α_p (ST at 760°C) has a fracture strain of about 0.33 compared to 0.23 for an equivalent microstructure with elongated α_p. In the β-ST plus α-aged conditions with no primary α the ductilities at comparable yield stresses are the same in both forgings as expected. It should be noted, however, that identical heat treatments for both forgings resulted in different yield stresses. The pancake showed a lower yield stress in the β-ST plus α-aged condition (compare conditions V and VII in Table 1) and a higher yield stress (100MPa) after solution treating at 760°C and aging at 500°C for 1 hr. This opens the question of whether or not this difference is due to a texture effect or, more importantly, can the ductility difference between microstructures with globular and elongated primary α at a constant yield stress be solely attributed to the difference in α_p-morphology. 5) ω-aging to a yield stress around 1250MPa ($\sim$181 ksi) results in very low ductilities (1–2% reduction in area) compared to all α-aged conditions. At lower yield stresses ($\sim$ 1050MPa) the ductility increases considerably and is comparable to that of a microstructure with 30% primary α.

III. Fractography

Fractographic studies of some of the microstructures by scanning electron microscopy revealed some qualitative explanations for the tensile test results. At least three different types of fracture topography have been observed, as shown in Figure 6.

The ($\alpha+\beta$) ST plus α-aged conditions show a complex dimple rupture fracture mode (Fig. 6a). The size of the most obvious dimple is comparable to the spacing of the α_p, but there are also much smaller dimples (< 1μm) present for several microstructures; these are possibly related to the secondary α.

The β-ST and α-aged microstructures especially in the high strength condition ($\sigma_{0.2}$ > 1300 MPa) show mainly intergranular fracture (Fig. 6b). Very small dimples (< 1μm) have been observed on the grain boundary facets. With decreasing yield stress the amount of intergranular fracture decreases and, instead, more transgranular dimple type fracture is observed (Fig. 6c). This dimple fracture is rather irregular with small dimples in the range of 1μm or less and a coarser structure in the range of 10-15μm.

Figure 6d illustrates the fracture of an ω-aged microstructure (β-ST + ω-aged, RA = 0%). It shows the line of intersection between the specimen surface and the fracture surface. It is apparent that very intense slip bands have formed in the ω-aged matrix, and fracture occurred along these slip bands.

Discussion

The results have shown that a variation in heat treatment at a constant

forging history can lead to a wide variety of microstructures in Ti-10-2-3. The main microstructural variables were the α_p volume fraction, the secondary α volume fraction and morphology and the grain boundary α. Also, on selected microstructures the α_p morphology has been varied (elongated instead of globular) by a different forging history. Also, a limited number of ω-aged conditions have been studied. Based on the mechanical properties for different combinations of these parameters (Fig. 5) we will discuss some more macroscopic aspects of an optimum microstructure. We also will offer some thoughts which may help to understand the microscopic mechanisms of strengthening and fracture.

For all the groups of microstructures (constant volume fraction of α_p), it is possible to produce a wide range of yield stresses. Increasing the aging temperature would extend the yield stress range to still lower values. If only an optimum combination of yield stress and ductility is desired, it seems most appropriate to take a microstructure with very little α_p (Fig. 5). However, fatigue properties as well as fracture toughness or corrosion properties usually have to be taken into account in structural design. Thus, other microstructures with comparable yield stresses remain interesting because they may be superior with respect to other properties.

A preliminary explanation of the different ductilities for the various groups of microstructures is possible based on the fracture surface studies (Fig. 6).

The relatively low ductilities of the β-ST and α-aged conditions compared to the $(\alpha+\beta)$ ST plus α-aged conditions can be attributed to a difference in fracture mode. As has been shown earlier[14], the long, soft grain boundary α layers deform preferentially which leads to a high plastic deformation in a very small volume before the yield stress of the matrix is reached. Because of the long slip length, stress concentrations form at grain boundary triple points where the slip is stopped. This can lead to fracture at very low macroscopic strains, although locally a high plastic deformation occurs. On a Ti-Mo alloy it has been shown that reducing the length of those soft zones by a smaller grain size can considerably increase the ductility by lowering the stress concentrations at the triple points[14]. It may be useful to try this also with Ti-10-2-3.

In the ω-aged microstructures the ω-particles are sheared. Intense slip bands form which create high stress concentrations at grain boundaries or primary α-particles and can lead to early fracture. In an ω-aged β-Ti alloy it has been shown that a reduction in grain size improved the ductility significantly, because it reduced the stress concentrations at the grain boundaries by a smaller pile-up length[16]. Again, for the ω-aged conditions a test with a smaller grain size seems to be useful in order to improve ductility.

The $(\alpha+\beta)$ ST plus α-aged conditions are of special interest, as they are commercially most interesting. Although a useful discussion of microscopic deformation and fracture is not possible from the present data, we do want to mention some factors which we think are important. For example, varying the volume fraction of α_p changes the matrix composition. This in turn results in different volume fractions and possibly different morphologies of the secondary α for a certain aging treatment. Assuming that both types of α can play a role in the fracture process, it is quite difficult to separate their contributions. In addition, one has to consider that the α-phase is

softer than the aged matrix and begins to deform plastically at lower stress-
es. Thus, for an increasing volume fraction of α_p the matrix has to be
hardened more strongly in order to achieve the same macroscopic yield stress
for such a microstructure compared to one with less primary α. As both types
of α have been changed, again their contributions to fracture have to be
separated. Consequently it appears to be promising to study the micromechan-
isms of deformation and fracture in more detail, which we already started on
the basis of the present results.

Conclusions

In Ti-10-2-3 a variety of aged microstructures with different volume
fractions and morphologies of primary and secondary α and also grain boundary
α has been tensile tested. The results can be summarized as follows:

1) For a constant volume fraction of primary α it is possible to vary
   the yield stress in a wide range; it is also possible to reach
   comparable yield stress levels for different volume fractions of α_n
   by an appropriate choice of aging temperatures and times as well
   as heating up rates to the aging temperatures.

2) Increasing the volume fraction of primary α reduces the ductility
   at comparable yield stresses for the α-aged conditions. Only the
   β-ST conditions with no primary α are an exception. They have
   lower ductilities than the $(\alpha+\beta)$ ST conditions. The ω-aged
   microstructures have the lowest ductilities at comparable yield
   stresses.

3) The differences in ductilities between the $(\alpha+\beta)$ ST and α-aged,
   the β-ST and α-aged and the ω-aged microstructures are qualita-
   tively related to different fracture modes.

4) Microstructures from a different forging which instead of the
   above tested globular primary α have elongated primary show lower
   ductilities at comparable yield stresses.

Acknowledgments

References

1. E. Bohanek: "Titanium Science and Technology," Vol. 3, Plenum Press,
    New York, (1973), 1983.
2. F. H. Froes, J. C. Chesnutt, C. G. Rhodes, and J. C. Williams: ASTM,
    STP 651, "Toughness and Fracture Behavior of Titanium," (1978), 115.
3. F. H. Froes, R. F. Malone, V. C. Peterson, C. G. Rhodes, J. C. Chesnutt,
    and J. C. Williams: AFML-TR-75-4, Vols I and II, Air Force Materials
    Laboratory, Dayton, OH, 1975.
4. J. C. Williams, F. H. Froes, J. C. Chesnutt, C. G. Rhodes, and R. G.
    Berryman: ASTM, STP 651, "Toughness and Fracture Behavior of Titanium,"
    (1978), 64.

5. H. W. Rosenberg: Joint Conference: Forging and Properties of Aerospace
    Materials, University of Leeds, January 1977.
6. E. Bohanek: Titanium Metals Corporation of America, Technical Report
    Number 55, May 1972.
7. C. C. Chen and C. P. Gure: Report RD74-120, Wyman-Gordon Company, North
    Grafton, MA, November 1974.
8. C. C. Chen: Report RD-75-118, Wyman-Gordon Company, North Grafton, MA,
    November 1975.
9. R. R. Boyer, J. W. Tripp, and J. E. Magnuson: presented at the TMS-AIME
    Fall Meeting, Milwaukee, WI, September 1978.
10. C. C. Chen and R. R. Boyer: J. of Metals, 31 (1979), 33.
11. G. Lenning: RD 012, TIMET, March 1976.
12. I. A. Matwell: AFML-TR-78-114, Air Force Materials Laboratory, Dayton,
    OH, 1978.
13. T. Hamajima, G. Luetjering, and S. Weissman: Met. Trans. 4 (1973), 847.
14. M. Peters and G. Luetjering: Zeitschift f. Metallkunde, 67 (1976), 811.
15. M. G. Mendiretta, G. Luetjering, and S. Weissman: Met. Trans., 2 (1971),
    2599.
16. A. Gysler, G. Terlinde, and G. Luetjering: Proc. 3rd Int. Conf. on
    Titanium, Moscow, 1976.
17. J. C. Chesnutt and F. H. Froes: Met. Trans., 8A (1977), 1013.
18. J. C. Williams, B. S. Hickman, and H. L. Marcus: Met. Trans., 2 (1971),
    1913.
19. T. W. Duerig, G. T. Terlinde, and J. C. Williams: Phase Transformations
    and Tensile Properties of Ti-10V-2Fe-3Al, Met. Trans. (in press).

Table 1 Mechanical properties of selected microstructures in Ti-10-2-3

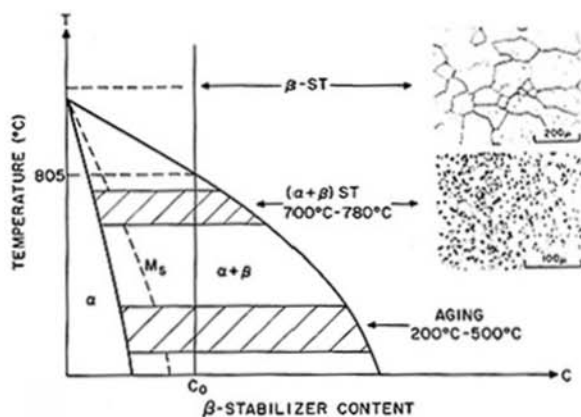|	Condition	Heat Treatment	Microstructure	$\sigma_{0.2}$ (MPa)	UTS (MPa)	e_g (%)	ε_F
Globular prim.α	I	725°C 20 hrs, WQ + 500°C 1 hr(salt)	30% prim.α + "large" sec. α	1063	1106	17.7	0.99
	II	725°C 100 min. WQ + 370°C 10^3 min.	30% prim.α + "small" sec. α	1246	1419	7.6	0.19
	III	780°C 3 hrs WQ + 500°C 1 hr (salt)	10% prim.α + "large" sec. α	1202	1247	10.3	0.63
	IV	780°C 3 hrs WQ + 500°C 1 hr (air)	10% prim.α + "small" sec. α	1445	1544	2.4	0.09
	V	850°C 2 hrs WQ + 500°C 4 hrs (salt)	0% prim.α + grain bound.α + "large" sec. α	1250	1308	3.9	0.16
Elongated prim. α	VI	700°C 8 hrs WQ + 200°C 6800 min.	35% prim.α + ω	1218	1266	0.5	0.02
	VII	850°C 2 hrs WQ + 500°C 4 hrs (salt)	0% prim.α + "large" sec. α + grain bound. α	1182	1265	3.8	0.17
	VIII	760°C 75 min. WQ + 500°C 1 hr (salt)	∿10% prim.α + "large" sec. α	1298	1381	4.6	0.23
	IX	700°C 75 min. WQ + 350°C 10^3 min.	∿30% prim.α + "small" sec.α	1239	1395	3.9	0.11

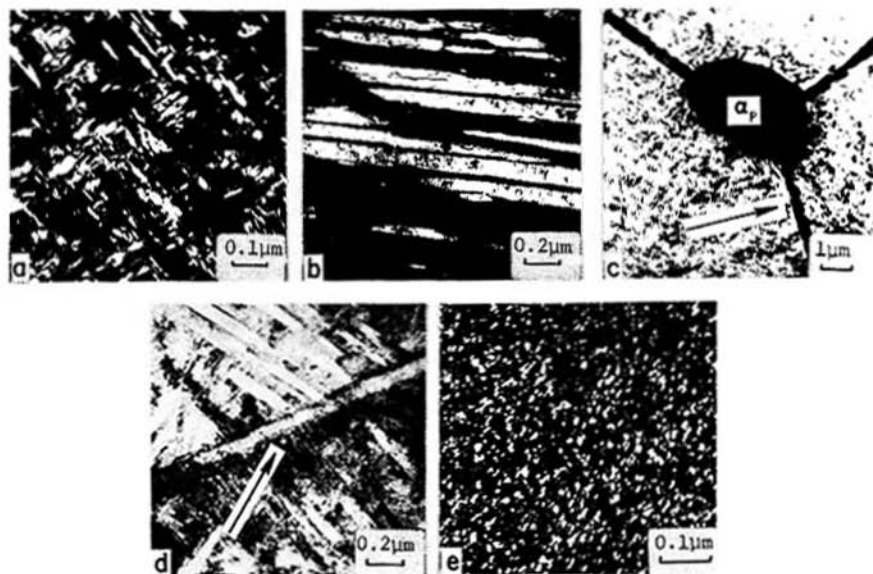Fig. 1 - Schematic phase diagram with solution treated microstructures and heat treatment temperature ranges.

Fig. 2 - Aging products in Ti-10-2-3
a) "Fine" secondary α, which follows metastable ω (TEM darkfield)
b) "Large" secondary α, which forms autocatalytically (TEM darkfield)
c) Subgrain boundary α (TEM brightfield)
d) Grain boundary α (TEM brightfield)
e) ω-phase (TEM darkfield)

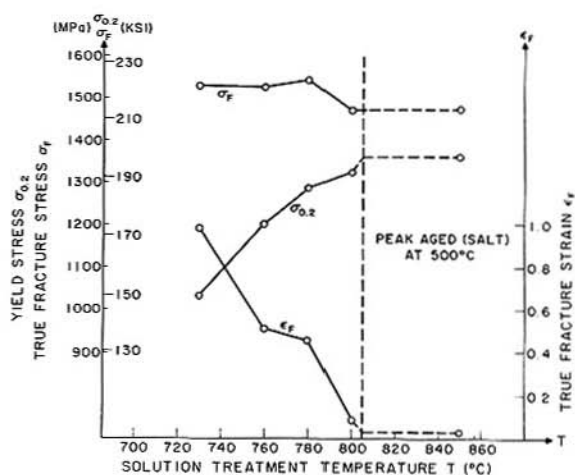Fig. 3 - Yield stress $\sigma_{0\cdot2}$, true fracture stress σ_F and true fracture strain ϵ_F as a function of ST temperature for specimens aged to maximum strength at 500°C.
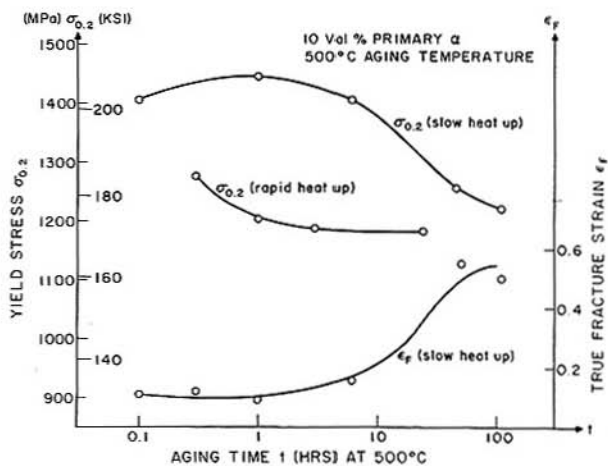

Fig. 4 - Yield stress $\sigma_{0\cdot2}$ and true fracture strain ϵ_F for microstructure with 10% α_ρ isothermally aged at 500°C.
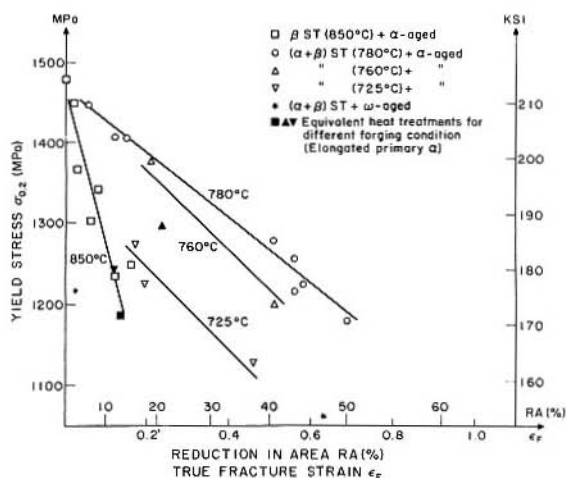
Fig. 5 – Relation between yield stress and true fracture strain ε_F or reduction in area RA, respectively, for various microstructures.
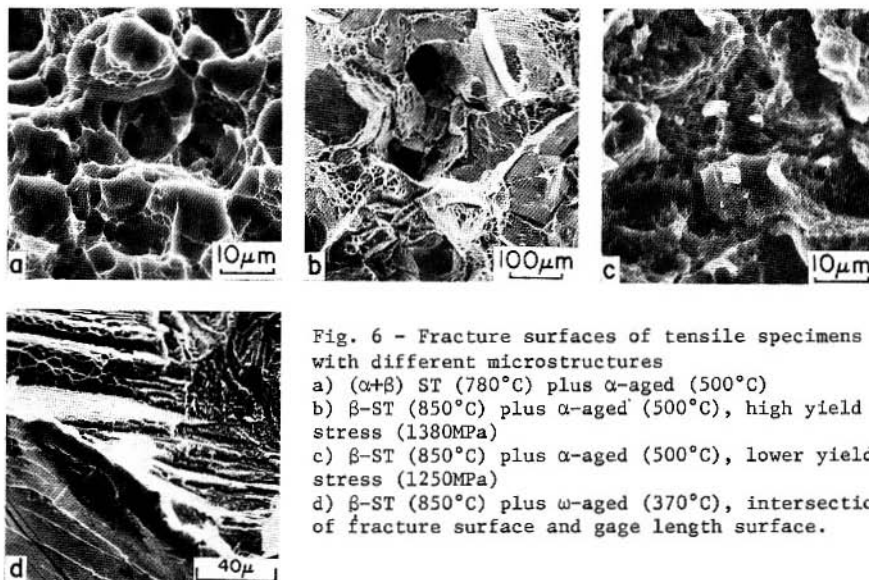

Fig. 6 – Fracture surfaces of tensile specimens with different microstructures
a) $(\alpha+\beta)$ ST (780°C) plus α-aged (500°C)
b) β-ST (850°C) plus α-aged (500°C), high yield stress (1380MPa)
c) β-ST (850°C) plus α-aged (500°C), lower yield stress (1250MPa)
d) β-ST (850°C) plus ω-aged (370°C), intersection of fracture surface and gage length surface.